Entropically Patchy Particles: Engineering Valence through Shape Entropy

Greg van Anders,[†] N. Khalid Ahmed,[†] Ross Smith,[‡] Michael Engel,[†] and Sharon C. Glotzer[†,‡,*]

[†]Department of Chemical Engineering and [‡]Department of Materials Science and Engineering, University of Michigan, Ann Arbor, Michigan 48109-2136, United States

ABSTRACT Patchy particles are a popular paradigm for the design and synthesis of nanoparticles and colloids for self-assembly. In "traditional" patchy particles, anisotropic interactions arising from patterned coatings, functionalized molecules, DNA, and other enthalpic means create the possibility for directional binding of particles into higher-ordered structures. Although the anisotropic geometry of nonspherical particles contributes to the interaction patchiness through van der Waals, electrostatic, and other interactions, how particle shape contributes entropically to self-assembly is only now beginning to be understood. The directional nature of entropic forces has recently been elucidated. A recently proposed theoretical framework that defines and quantifies directional entropic forces demonstrates the anisotropic—that is, patchy—nature of these emergent, attractive forces. Here we introduce the notion of entropically patchy particles as the entropic counterpart to enthalpically patchy particles. Using three example "families" of shapes, we show how to modify entropic patchiness by introducing geometric features to the particles *via* shape operations so as to target specific crystal structures assembled here with Monte Carlo simulations. We quantify the emergent entropic valence *via* a potential of mean force and torque. We show that these forces are on the order of a few k_BT at intermediate densities below the onset of crystallization. We generalize these shape operations to shape anisotropy dimensions, in analogy with the anisotropy dimensions introduced for enthalpically patchy particles. Our findings demonstrate that entropic patchiness and emergent valence provide a way of engineering directional bonding into nanoparticle systems, whether in the presence or absence of additional, non-entropic forces.

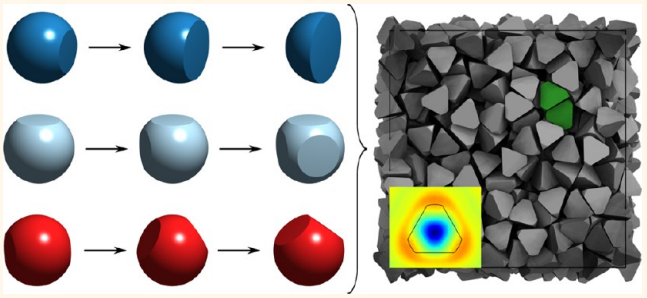

KEYWORDS: shape entropy · patchy particles · superlattices

Patchy particles[1,2] self-assemble into nanoparticle superlattices and colloidal crystals by exploiting anisotropic interactions arising from, for example, molecular patterning, DNA functionalization, and charge heterogeneity. Examples of patchy particles include Janus colloids,[3−9] striped nanospheres[10] and nanorods,[11] and DNA-coated patchy particles,[12] among many others.[2,13] When the particles are not spheres, non-isotropic van der Waals and other forces also contribute to interaction patchiness. With patchy particles, anisotropically placed patches promoting either specific or nonspecific interactions with patches on other particles induce directional "bonding" between particles of the sort typically attributed to molecular substances. To date, patchy particles have been assembled into numerous structures,[14−24] many of them isostructural to their atomic and molecular counterparts.

Recently, there has been considerable focus on the contribution of entropic forces to the assembly of anisotropically shaped particles into complex structures.[25−44] A general observation from many of these studies is that dense suspensions of hard, faceted particles align their facets so as to maximize the system entropy, giving rise to ordered structures as complex as colloidal quasicrystals[29,35] and crystals with unit cells containing as many as 52 particles.[36] Damasceno *et al.*[35,36] rationalized this tendency toward facet alignment as the emergence of "directional entropic forces" between hard particles. Directional entropic forces (DEFs) are not intrinsic to the particles but instead are statistical and emerge from the collective behavior of the entire system upon crowding. The DEF approach to the self-assembly of colloidal cubes, octahedra, rhombic dodecahedra, and tetrahexahedra was recently demonstrated by Young *et al.*[45]

* Address correspondence to sglotzer@umich.edu.

Received for review November 4, 2013 and accepted December 21, 2013.

Published online December 21, 2013
10.1021/nn4057353

A theoretical framework for the description and quantification of DEFs was proposed recently.[46] Using an effective potential of mean force and torque (PMFT), hard polyhedra, spherocylinders, and hemispheres were shown to exhibit spatially anisotropic probability distributions describing the likely positions of neighboring particles, much like the polyvalent nature of molecules. Unlike in molecular systems, however, here the valence is density-dependent and—because it arises statistically from collective behavior—is emergent. We define these emergent valence regions of effective attraction between particles as "entropic patches". These patches can achieve strengths of several to many k_BT, aligning complementary geometrical features just as enthalpically patchy particles align complementary enthalpic features.

Here we introduce the notion of entropically patchy particles as the entropic counterpart to enthalpically patchy particles, and we show how DEFs can be engineered through the systematic alteration of particle shape to target specific self-assembled structures. Using three example families of shapes, we systematically apply certain shape operations to the particles so as to modify entropic patchiness to be consistent with target crystal structures. In contrast to the charge, chemical, *etc*. mediation of the interaction between sticky patches on *enthalpically* patchy particles, attractive *entropic* patches are features in particle shape that promote local dense packing in thermodynamic equilibrium. We show that we indeed obtain these structures through self-assembly with Monte Carlo (MC) simulations. We generalize these shape operations to shape anisotropy dimensions, in analogy with the anisotropy dimensions introduced for patchy particles.[2] Our findings demonstrate the utility of the notions of entropic patchiness and emergent valence as an additional way of engineering directional bonding into nanoparticle systems, whether in the presence or absence of additional, non-entropic forces.

Background. The PMFT, F_{12}, describing the directional entropic force between a pair of hard particles in a system of identical particles has been derived[46] as

$$F_{12}(\Delta\xi_{12}) = -k_BT \log(H(d(\Delta\xi_{12}))J(\Delta\xi_{12})) + \tilde{F}_{12}(\Delta\xi_{12}) \quad (1)$$

Here, $\Delta\xi_{12}$ describes the relative position and orientation of the particle pair. H is the Heaviside step function, and $d(\Delta\xi_{12})$ is the minimum separation distance of the particle pair in their relative position and orientation, which is negative when the particles overlap and positive when they do not. J is the Jacobian for the set of invariant coordinates of interest for a particular problem. $\tilde{F}_{12}$ is the Helmholtz free energy available to other particles in the system when the relative position and orientation of the pair is fixed.

From eq 1, the PMFT can be seen to arise as a competition between two terms. The term coming from $\tilde{F}_{12}$ is determined by the free energy of the system with the pair fixed. If there is no intrinsic attraction among the particles, then this term will tend to induce a locally denser packing for the particle pair. The other contribution comes from the preference of the pair itself for a particular relative position and orientation. $\tilde{F}_{12}$ will be minimized when the particle pair aligns itself to maximize its local packing density according to the shape of the particles. The features of particle shape that facilitate locally dense packing, therefore, act as the "source" of the emergent attractive DEFs. We refer to these features as entropic patches.

RESULTS AND DISCUSSION

Targeted Self-Assembly through Emergent Valence. We design entropic patches to self-assemble the following target structures: simple cubic, body-centered cubic (bcc), diamond, and dodecagonal quasicrystal. Each of these has been reported in experiments or simulations of patchy spheres or hard polyhedra. In all cases, the local coordination shell at least partially dictates the type of crystal structure that assembles.[36] We attempt to create similar local coordination shells through entropic patches engineered by slicing facets into hard spheres. Specifically, we simulate spheres with cubic, octahedral, and tetrahedral faceting to induce the appropriate entropic patchiness and show that at sufficient crowding the desired valence emerges, leading to crystallization of target structures consistent with that particular polyvalent coordination *via* the organization of successive neighbor shells.

We first target the assembly of a (tetrahedrally coordinated) diamond lattice by tetrahedrally faceting spheres. The diamond lattice has been assembled in simulation by decorating a sphere with four tetrahedrally coordinated enthalpic patches (sticky spots).[1,47] We therefore "slice" four equal sized facets into a sphere at the locations of the faces of a regular tetrahedron. We consider a faceting amount of $\alpha = 0$ to be a perfect sphere and $\alpha = 1$ to be a perfect tetrahedron. For concreteness, consider a tetrahedron with vertices at (1, 1, 1), (−1, −1, 1), (−1, 1, −1), and (1, −1, −1). A perfect sphere is the intersection of this tetrahedron with a sphere centered about the origin with radius $1/\sqrt{3}$. A perfect tetrahedron is the intersection of this tetrahedron and a sphere with radius $\sqrt{3}$. The radius of the sphere required to generate any amount of faceting α between these limits is given by the formula $1/\sqrt{3}(1 - \alpha) + \sqrt{3}\alpha$. We performed MC simulations of monodisperse systems of 1000 such particles at fixed volume, for several choices of α (see Methods for details). We computed the force component of the PMFT as a function of the Cartesian components of the separation vector of the particles in the frame of one of the particles. (A detailed description of the computation and a discussion of possible coordinate systems have been given elsewhere.[46])

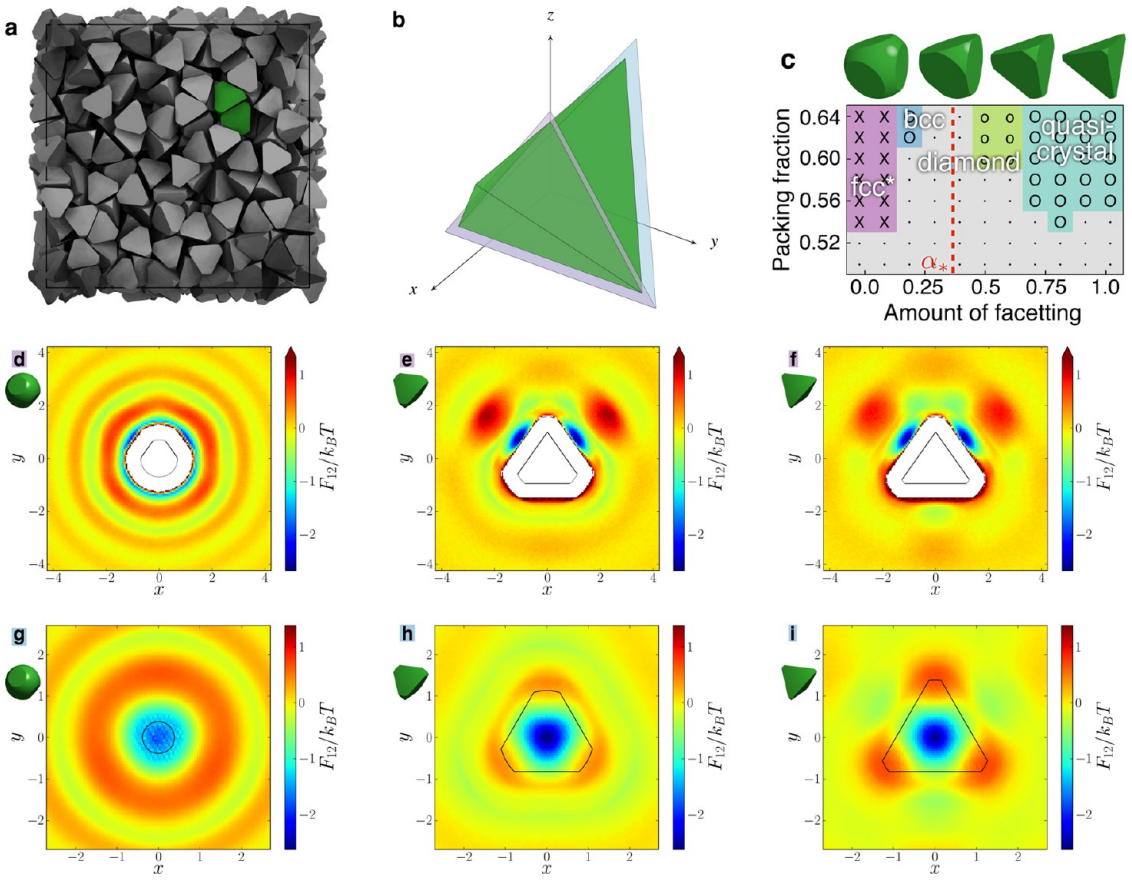

Figure 1. We demonstrate shape-induced entropic valence in monodisperse systems of hard tetrahedrally faceted spheres by computing the PMFT for a pair of particles in a system of 1000 particles at packing fraction 0.5 (a). Slicing the potential along two different planes (b) shows the induced valence in a plane through the facet (d−f) and a plane parallel to the facet (g−i). At sufficient crowding, the entropic forces arising from shape entropy lead to crystallization (c). As the faceting amount α increases from 0.1 (d,g), to 0.6 (e,h), to 0.8 (f,i), the PMFT shows greater evidence of shape-induced entropic valence that determines the crystal structure (face-centered cubic (fcc), diamond, and quasicrystal, respectively), even at insufficient crowding (50%) to provoke crystallization.

In Figure 1, we show that monodisperse, tetrahedrally faceted spheres manifest shape-induced entropic valence (*via* the PMFT) in dense fluids at 50% packing fraction. Simulations were performed at faceting amounts between a perfect sphere (α = 0) and a perfect tetrahedron (α = 1). (See Table 1 in Supporting Information for actual faceting amounts for this and other particles below.) At a faceting amount of α = 0.6, the particles self-assemble a diamond lattice in MC simulation at a packing fraction of 60% as shown in Figure 1c. Also note that when the faceting amount α exceeds

$$\alpha_* = \frac{\sqrt{3}-1}{2} \approx 0.3660254 \qquad (2)$$

(dashed red line in Figure 1c) the faceting patches share adjacent edges, which we would expect to have an effect on the local dense packing. Only above this faceting amount are we able to assemble the diamond lattice as shown in Figure 1c. Note that a family of moderately truncated tetrahedra also assemble a diamond lattice.[35]

As a second example, we next target simple cubic lattices by slicing cubically coordinated facets into hard spheres. We denote a perfect sphere as α = 0 and a perfect cube as α = 1. For concreteness, take the vertices of the cube to be at (1,1,1) and at similar locations in each of the other octants. A perfect sphere is the intersection of this cube with a sphere centered about the origin with unit radius. A perfect cube would be the intersection with a sphere of radius $\sqrt{3}$. The radius of the sphere required to generate any amount of faceting α between a cube and a sphere is given by the formula $1 + (\sqrt{3} - 1)\alpha$. In Figure 2, we show the role of the PMFT in generating directional entropic forces that cause particles to have high positional correlation at facet locations.

We compute the PMFT in a monodisperse system of hard cubically faceted spheres at a density of 50% (in the fluid phase) at faceting amounts of α = 0.2, 0.5, and 0.8 (see Supporting Information for other faceting amounts). We plot the PMFT in panels d−i, by slicing according to the diagram in Figure 2b with faceting amount α increasing from left to right. In panels d−f (labeled also with blue), we show slices of the PMFT at constant *z* as depicted by the blue plane in Figure 2b. (Here, we take $z \approx 0$.) In panels g−i (labeled also with

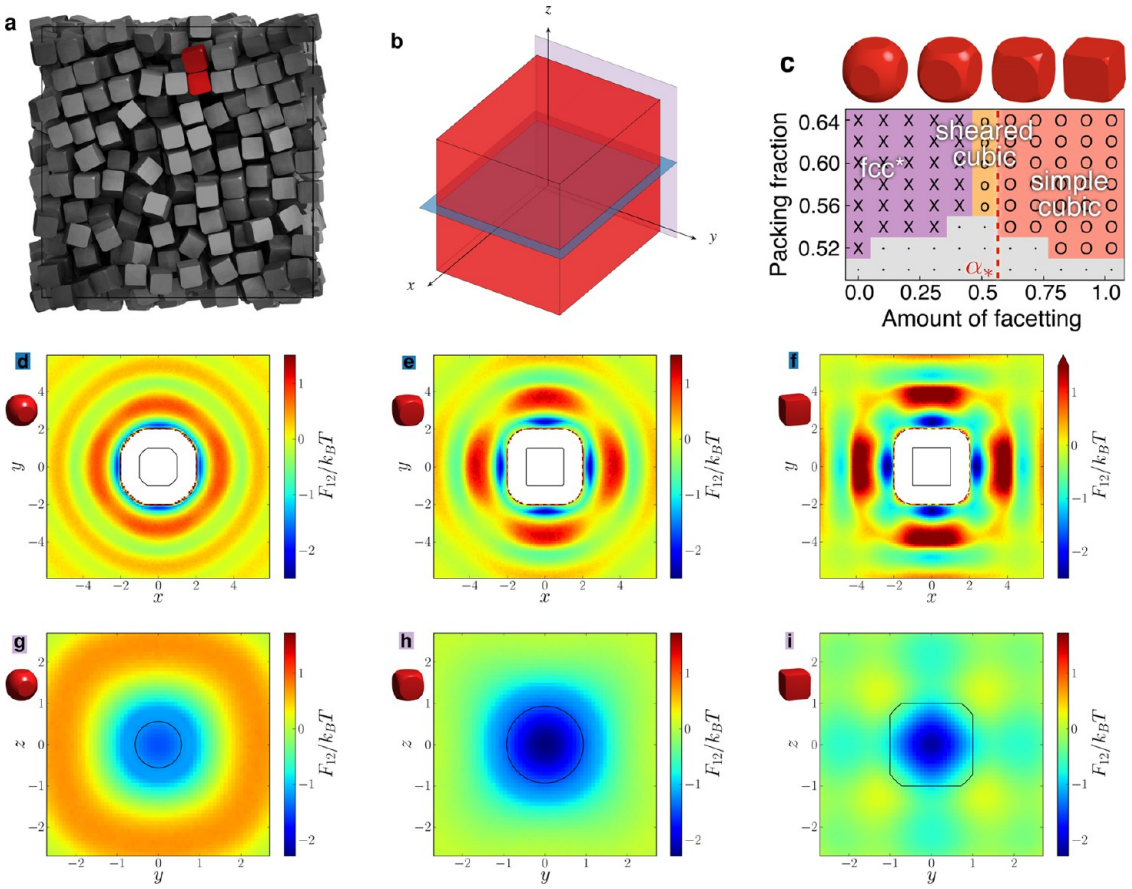

Figure 2. We demonstrate shape-induced entropic valence in monodisperse systems of hard cubically faceted spheres by computing the PMFT for a pair of particles in a system of 1000 particles at packing fraction 0.5 (a). Slicing the potential along two different planes (b) shows the induced valence in a plane through the facet (d−f) and a plane parallel to the facet (g−i). At sufficient crowding, the entropic forces arising from shape entropy lead to crystallization (c). As the faceting amount α increases from 0.2 (d,g), to 0.5 (e,h), to 0.8 (f,i), the PMFT shows greater evidence of shape-induced entropic valence that determines the crystal structure (fcc, sheared cubic, and simple cubic, respectively), even at insufficient crowding (50%) to provoke crystallization.

mauve), we slice the PMFT parallel to the faceting patch (the mauve plane in Figure 2b) through the minimum of the potential. We see that upon increasing the faceting amount we induce a greater amount of cubic coordination in the fluid at fixed density. At a faceting amount of $\alpha = 0.2$ (panels d and g), the PMFT is nearly isotropic, indicating that faceting plays only a small role in locally ordering the particles. However, at faceting amounts of $\alpha = 0.5$ (panels e and h) and $\alpha = 0.8$ (panels f and i), we observe PMFT differences on the order of 2−3 k_BT favoring alignment of facets. Simple cubic lattices (Figure 2c) assemble at $\alpha \approx 0.6$ or more in MC simulations at packing fractions of 54% or more. Note that when the faceting amount α exceeds

$$\alpha_* = \frac{\sqrt{2}-1}{\sqrt{3}-1} \approx 0.565826 \qquad (3)$$

(dashed red line in Figure 2c) the shape of the faceting patch goes from being circular to having four straight edges that are shared by adjacent patches. The existence of this edge should have an effect on the geometry of the locally preferred packing, and it is, perhaps, not surprising that above this faceting amount we observe the assembly of simple cubic lattices. The self-assembly of cubic, or nearly cubic, particles into simple cubic lattices has been seen before.[38,41]

As a final example, we target a bcc or sheared bcc crystal with eight nearest neighbors by octahedrally faceting a sphere. We denote a perfect sphere as $\alpha = 0$ and a perfect octahedron as $\alpha = 1$. For concreteness, take the vertices to lie at a unit distance from the origin along each of the Cartesian coordinate axes, at (1,0,0), (−1,0,0), *etc*. A perfect sphere is the intersection of this cube with a sphere centered about the origin with radius $1/\sqrt{3}$. A perfect octahedron is the intersection with a sphere of unit radius. The radius of the sphere required to generate any amount of faceting α between the sphere and the octahedron is given by the formula $1 + (1 - (1/\sqrt{3}))\alpha$. Simulations were performed at faceting amounts between these two limits. At low faceting amounts, where the entropic valence (patchiness) is fairly isotropic, the systems assembled fcc crystals. However, at faceting amounts as low as

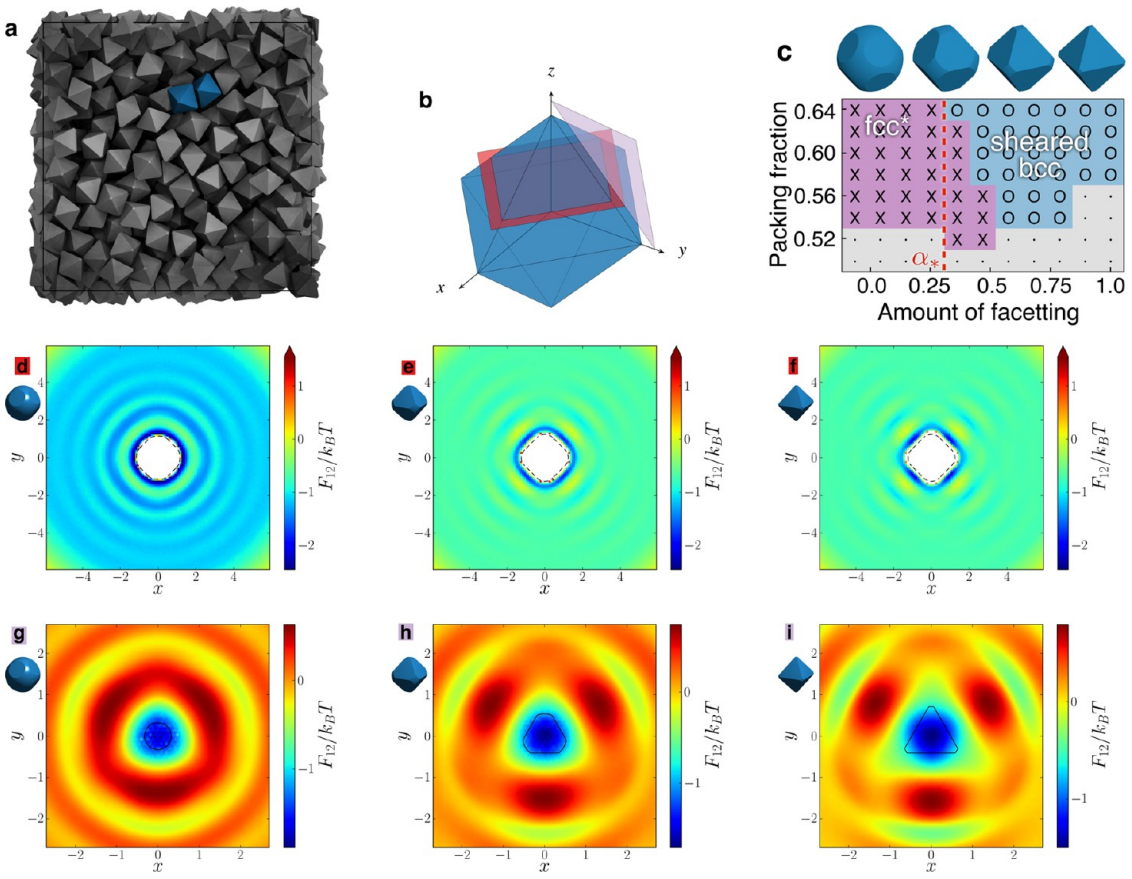

Figure 3. We demonstrate shape-induced entropic valence in monodisperse systems of hard octahedrally faceted spheres by computing the PMFT for a pair of particles in a system of 1000 particles at packing fraction 0.5 (a). Slicing the potential along two different planes (b) shows the induced valence in a plane through the facet (d−f) and a plane parallel to the facet (g−i). At sufficient crowding, the entropic forces arising from shape entropy lead to crystallization (c). As the faceting amount α increases from 0.2 (d,g), to 0.6 (e,h), to 0.8 (f,i), the PMFT shows greater evidence of shape-induced entropic valence that determines the crystal structure (fcc at 0.2 and sheared bcc at 0.6 and 0.8), even at insufficient crowding (50%) to provoke crystallization.

α = 0.4, we observe sheared bcc crystals. Note that when the faceting amount α exceeds

$$\alpha_* = \frac{\frac{\sqrt{3}}{\sqrt{2}} - 1}{\sqrt{3} - 1} \approx 0.307007 \qquad (4)$$

(dashed red line in Figure 3c) the faceting patches begin to share adjacent edges. This figure coincides with the lowest faceting amount at which we observed the sheared bcc crystal in our simulations. Octahedra have been studied previously,[35−38,43] where bcc and sheared bcc lattices were also observed. One interesting feature of the octahedrally faceted particles is that entropically preferred local dense packings have particles situated face-to-face, but with the orientation of the adjacent faces rotated by 180°. In the resulting "star of David" arrangement (see Supporting Information Figure S10), the protruding vertices reduce the free volume available to the surrounding particles. This means that although face-to-face arrangements are still favored by shape entropy, as exhibited in the increasing anisotropy of the PMFT depicted in Figure 3, the strength of the entropic patch is actually lessened at high degrees of faceting, compared with lower degrees.

Generalization and Anisotropy Dimensions. The angular specificity achieved by facet alignment *via* DEFs is reminiscent of the angular specificity of enthalpic interactions conceptualized within the patchy particle paradigm.[1,2] However, in contrast to the chemical or other patterning that leads to enthalpic patchiness, the angular specificity of interactions arises here solely due to entropic considerations arising from features in particle shape that promote local dense packing. These features act as "entropic patches" that cause preferential alignment. Beyond the simple faceting of hard spheres, there are many ways of altering particle shape to introduce patches that promote local dense packing.

The various shape operations that may be applied to generate attractive entropic patches may be described in terms of anisotropy dimensions (Figure 4), as was done for enthalpic patches.[2] Of course, in contrast to traditional sticky patches, entropic patchiness is an emergent, effective concept that depends not only on density but also on all geometric features within the

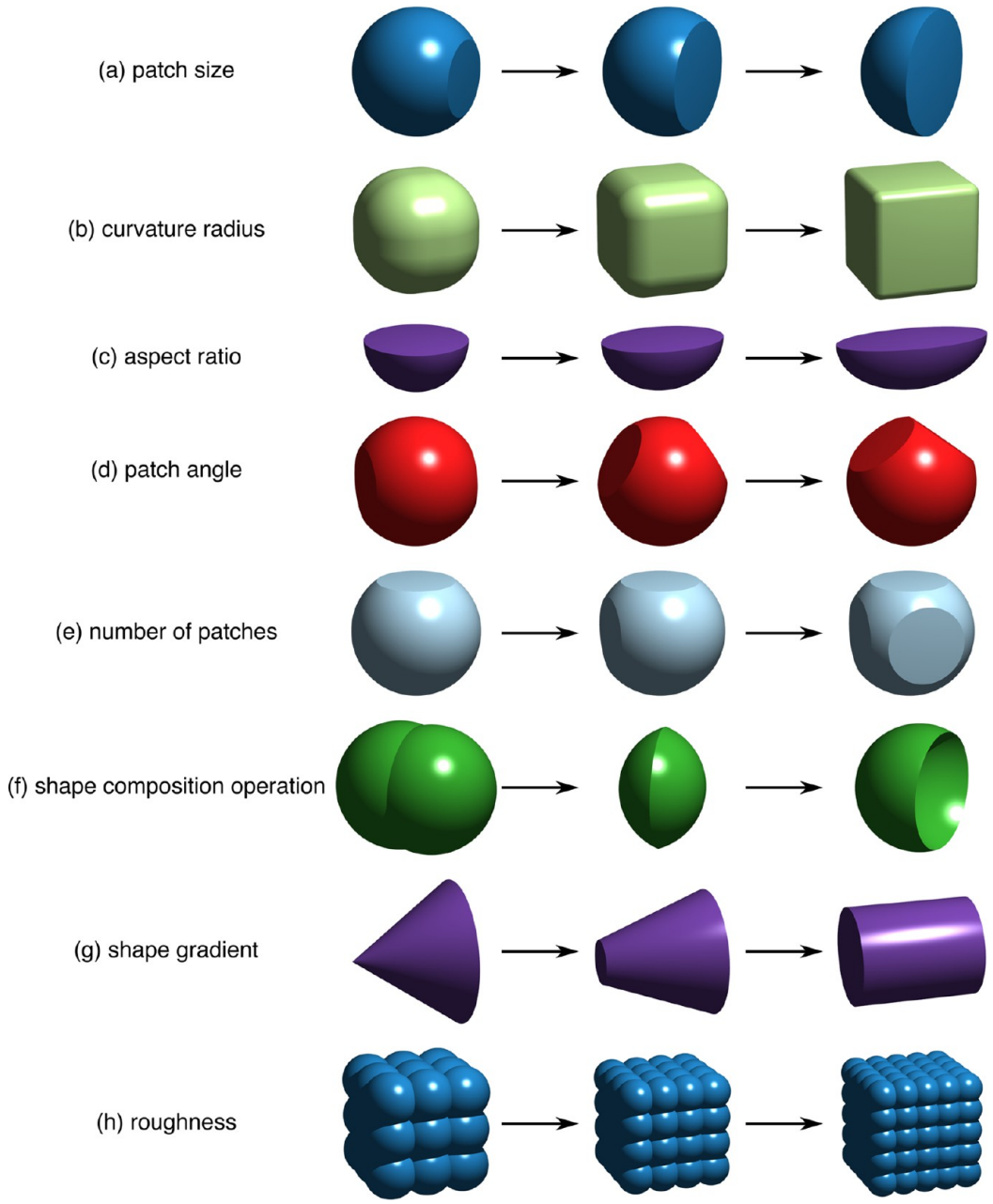

Figure 4. (a) Creation and altering of entropic patches can be conceptualized as anisotropy dimensions: (a) patch size, (b) curvature radius, (c) aspect ratio, and (d) patch angle, (e) number of patches, (f) shape composition operation, (g) shape gradient, and (h) roughness.

characteristic length of the interaction. Such features may include, for example, flat facets or other low curvature regions and interlocking or "mating" features. Conversely, high curvature regions could be used to introduce repulsive patches.

Eight examples of shape anisotropy dimensions are illustrated in Figure 4. Many of these anisotropy dimensions have already been explored in particles synthesized in the literature. For example, in lock-and-key colloids,[48] the anisotropy dimensions of patch size (a), curvature radius (b), and shape composition operation (f) have been synthesized.[49] In roughened colloids, the anisotropy dimensions of patch size (a), aspect ratio (c), patch angle (d), number of patches (e), and roughness (h) have been synthesized.[50−56] There are many other examples of work in the literature that can be considered explorations of these anisotropy dimensions.[45,57−86]

Shape anisotropy dimensions can be combined in different ways to yield various particles that have appeared in the literature, such as lock-and-key colloids[48,87] and various novel particle geometries. For example, in Figure 5, we consider applying the anisotropy dimension of number of patches to three different species of particle: roughened colloids,[50−56] faceted spheres, and dimpled spheres.[48,49,86] In Figure 6, we consider the shape space defined by the application of three

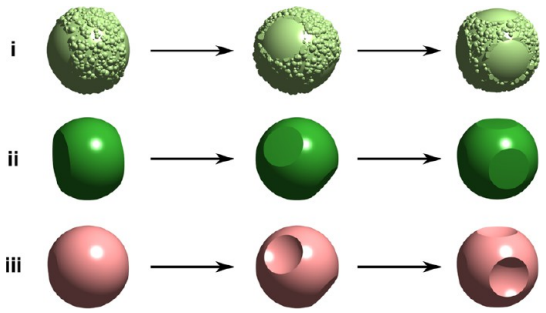

Figure 5. Schematic showing the same anisotropy dimension (e, number of patches) applied to three different particle types: (i) a roughened colloid, (ii) a faceted sphere, and (iii) a dimpled sphere.

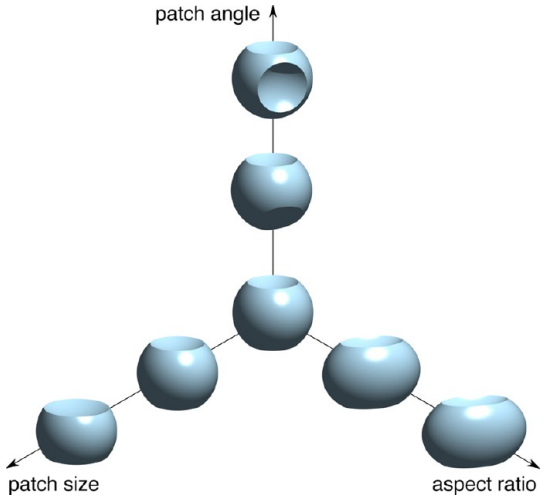

Figure 6. Schematic showing the result of combining various anisotropy dimensions by applying patch angle (d), aspect ratio (c), and patch size (a) from Figure 4 to a sphere with two "dimple" patches.

orthogonal anisotropy dimensions to the dimpled sphere. There are obvious synergies between the anisotropy dimensions for enthalpically patchy particles presented here and the more general anisotropy dimensions first proposed by Glotzer and Solomon.[2] For example, aspect ratio (c here, b there), shape gradient (g in both), and roughness (h in both) are present in both frameworks, whereas patch size (a here) is analogous to surface coverage (a there), and combining patch angle and number of patches (d and e here) gives faceting (c there). Examples of enthalpically patchy particles and their entropically patchy analogues are shown in Figure 7a. As depicted in Figure 7b, combining both enthalpic and entropic patchiness provides opportunities for enhancing particular desired particle alignment or produces competing forces that may give rise to structures of high complexity.

As a final note, we point out that entropically patchy particles are also relevant in systems with depletants since depletant-induced colloidal crystallization is controlled by the same entropic mechanism as the

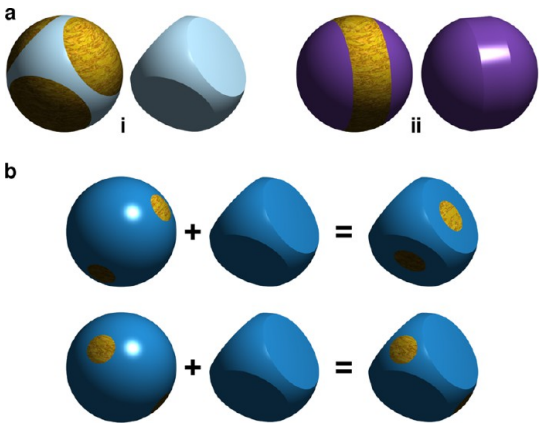

Figure 7. (a) Many anisotropy dimensions for enthalpically patchy particles[2] have entropically patchy counterparts. Examples of traditional sticky patchy particles left (i) and (ii) with entropically patchy counterparts right (i) and (ii). (b) Enthalpic patches can be combined with entropic patches to enhance or inhibit entropic patchiness as shown schematically here. This can be obtained by using the same direction for both types of patches (top) or by using different directions for the entropic patches and the enthalpic patches (bottom).

crystallization of hard colloids.[46] The interaction range for DEFs is determined by the scale of the particles being integrated out in the calculation of the PMFT. In traditional depletion systems, the depletants are typically much smaller than the colloids and penetrable. This hierarchy in scales produces a very short ranged interaction between nanoparticles or colloids, which allows for a clearer separation between geometric features on the colloids that contribute to local dense packing and thereby eases the identification of the features that are the entropic patches. Particularly salient examples of entropically patchy particles assembled through depletion forces include the work on selectively roughened colloids,[50−56] lock-and-key colloids,[48,49,86−89] and polyhedrally shaped metal nanoparticles,[37,45] each of which exploits geometrical features to create anisotropy in entropic interactions. These and related works have been reviewed elsewhere.[90]

CONCLUSION

We showed in three example model systems that by judiciously engineering particle shape we can induce angularly specific interactions between hard particles strong enough and directional enough to induce the self-assembly of a targeted crystal structure. In example systems, DEFs cause effective attractive interactions that are on the order of a few k_BT; such "bond" strengths are not atypical of enthalpically patchy particles at intermediate densities below the onset of crystallization. The DEFs responsible for ordering can be measured experimentally using, for example, optical tweezers and existing confocal microscopy techniques.[76,91] We abstracted these examples of particle

design to be part of a much broader method of shape engineering through entropic patches that serves to provide a means of self-assembling materials through entropic interactions alone. We introduced anisotropy dimensions to exhibit and organize the various ways in which particle shape can be engineered to exploit this method of realizing complex structures.

When combined with traditional enthalpic patchiness, entropic patchiness greatly enlarges the already vast design space for new nano- and micrometer-scale building blocks. The theoretical framework based upon the PMFT[46] allows the quantitative assessment of the relative strength of entropic driving forces for assembly when other forces also contribute. At the nanoscale, particles are seldom solely hard.[92] However, the fact that DEFs cause attractive interactions on the order of a few k_BT at intermediate packing densities that are easily experimentally accessible suggests there might be a large class of systems in which electrostatic or other forces can be sufficiently controlled such that entropic patches supply the dominant force controlling their self-assembly, as was demonstrated recently.[45,93,94] When enthalpic interactions tend to drive facet alignment anyway, as in, ligand-coated faceted nanoparticles,[94,95] the entropic contribution will only enhance that tendency.

METHODS

To measure the PMFT, we performed MC simulations of dense fluids of 1000 hard faceted spheres at fixed volume. We note[46] that the PMFT can be defined implicitly from the partition function

$$\mathcal{Z} = \int \mathrm{d}(\Delta\xi_{12}) e^{-\beta F_{12}(\Delta\xi_{12})} \quad (5)$$

In this form, the PMFT can be seen to be the logarithm of the integrand of the partition function. We computed the PMFT by examining the displacement between particles, which we computed in the coordinate frame of each particle and partitioned into defined regions. The orientations of the second particle were integrated over so as to sufficiently reduce the dimensionality of the potential to allow direct visualization. The possible relative positions of the particles were subdivided into a number of regions, and the PMFT was computed by observing the relative frequency of observing a pair of particles in each of these regions, as indicated in eq 5. Errors quoted are standard errors of the mean of independent runs of independently equilibrated systems. Full details on the source and analysis of numerical errors that can arise in computing DEFs can be found elsewhere.[46]

The MC method above, and for the results shown in Figures 1,2, and 3, employed single particle moves for both translation and orientation. In all cases, the simulation box was taken to be periodic and the volume fixed. However, for Figures 1c, 2c, and 3c, the box was permitted to shear at fixed volume. Overlaps were checked using the same implementation of the GJK algorithm[96] used in other work by some of the present authors.[36]

Conflict of Interest: The authors declare no competing financial interest.

Acknowledgment. We thank D. Klotsa and B. Schultz for helpful suggestions. This material is based upon work supported by, or in part by, the U.S. Army Research Office under Grant Award No. W911NF-10-1-0518, the DOD/ASD(R&E) under Award No. N00244-09-1-0062, and the Biomolecular Materials Program of the Materials Engineering and Science Division of Basic Energy Sciences at the U.S.Department of Energy under Grant No. DE-FG02-02ER46000. The calculations of the hard particle PMFT were supported by ARO. The development of the PMFT and anisotropy dimensions was supported by DoE. Any opinions, findings, and conclusions or recommendations expressed in this publication are those of the author(s) and do not necessarily reflect the views of the DOD/ASD(R&E).

Supporting Information Available: Supporting figures and table. This material is available free of charge via the Internet at http://pubs.acs.org.

REFERENCES AND NOTES

1. Zhang, Z.; Glotzer, S. C. Self-Assembly of Patchy Particles. *Nano Lett.* **2004**, *4*, 1407–1413.
2. Glotzer, S. C.; Solomon, M. J. Anisotropy of Building Blocks and Their Assembly into Complex Structures. *Nat. Mater.* **2007**, *6*, 557–562.
3. Paunov, V.; Cayre, O. Supraparticles and "Janus" Particles Fabricated by Replication of Particle Monolayers at Liquid Surfaces Using a Gel Trapping Technique. *Adv. Mater.* **2004**, *16*, 788–791.
4. Cayre, O.; Paunov, V. N.; Velev, O. D. Fabrication of Asymmetrically Coated Colloid Particles by Microcontact Printing Techniques. *J. Mater. Chem.* **2003**, *13*, 2445–2450.
5. Roh, K.-H.; Martin, D. C.; Lahann, J. Biphasic Janus Particles with Nanoscale Anisotropy. *Nat. Mater.* **2005**, *4*, 759–763.
6. Zhang, G.; Wang, D.; Möhwald, H. Patterning Microsphere Surfaces by Templating Colloidal Crystals. *Nano Lett.* **2005**, *5*, 143–146.
7. Cui, J.-Q.; Kretzschmar, I. Surface-Anisotropic Polystyrene Spheres by Electroless Deposition. *Langmuir* **2006**, *22*, 8281–8284.
8. Hong, L.; Jiang, S.; Granick, S. Simple Method To Produce Janus Colloidal Particles in Large Quantity. *Langmuir* **2006**, *22*, 9495–9499.
9. Zhang, Q.; Lee, Y. H.; Phang, I. Y.; Pedireddy, S.; Tjiu, W. W.; Ling, X. Y. Bimetallic Platonic Janus Nanoparticles. *Langmuir* **2013**, *29*, 12844–12851.
10. Jackson, A. M.; Myerson, J. W.; Stellacci, F. Spontaneous Assembly of Subnanometre-Ordered Domains in the Ligand Shell of Monolayer-Protected Nanoparticles. *Nat. Mater.* **2004**, *3*, 330–336.
11. Martin, B. R.; Dermody, D. J.; Reiss, B. D.; Fang, M.; Lyon, L. A.; Natan, M. J.; Mallouk, T. E. Orthogonal Self-Assembly on Colloidal Gold−Platinum Nanorods. *Adv. Mater.* **1999**, *11*, 1021–1025.
12. Wang, Y.; Wang, Y.; Breed, D. R.; Manoharan, V. N.; Feng, L.; Hollingsworth, A. D.; Weck, M.; Pine, D. J. Colloids with Valence and Specific Directional Bonding. *Nature* **2012**, *491*, 51–55.
13. Pawar, A. B.; Kretzschmar, I. Fabrication, Assembly, and Application of Patchy Particles. *Macromol. Rapid Commun.* **2010**, *31*, 150–168.
14. Park, S.; Lim, J.-H.; Chung, S.-W.; Mirkin, C. A. Self-Assembly of Mesoscopic Metal-Polymer Amphiphiles. *Science* **2004**, *303*, 348–351.
15. Li, F.; Yoo, W. C.; Beernink, M. B.; Stein, A. Site-Specific Functionalization of Anisotropic Nanoparticles: From Colloidal Atoms to Colloidal Molecules. *J. Am. Chem. Soc.* **2009**, *131*, 18548–18555.
16. Onoe, H.; Matsumoto, K.; Shimoyama, I. Three-Dimensional Sequential Self-Assembly of Microscale Objects. *Small* **2007**, *3*, 1383–1389.
17. Figuerola, A.; Franchini, I. R.; Fiore, A.; Mastria, R.; Falqui, A.; Bertoni, G.; Bals, S.; Van Tendeloo, G.; Kudera, S.; Cingolani, R.; *et al.* End-to-End Assembly of Shape-Controlled Nanocrystals *via* a Nanowelding Approach Mediated by Gold Domains. *Adv. Mater.* **2009**, *21*, 550–554.

18. Rycenga, M.; McLellan, J. M.; Xia, Y. Controlling the Assembly of Silver Nanocubes through Selective Functionalization of Their Faces. *Adv. Mater.* **2008**, *20*, 2416–2420.
19. Zhang, G.; Wang, D.; Möhwald, H. Decoration of Microspheres with Gold Nanodots: Giving Colloidal Spheres Valences. *Angew. Chem., Int. Ed.* **2005**, *44*, 7767–7770.
20. Gangwal, S.; Pawar, A.; Kretzschmar, I.; Velev, O. D. Programmed Assembly of Metallodielectric Patchy Particles in External AC Electric Fields. *Soft Matter* **2010**, *6*, 1413–1418.
21. Chen, Q.; Bae, S. C.; Granick, S. Directed Self-Assembly of a Colloidal Kagome Lattice. *Nature* **2011**, *469*, 381–384.
22. Chen, Q.; Whitmer, J. K.; Jiang, S.; Bae, S. C.; Luijten, E.; Granick, S. Supracolloidal Reaction Kinetics of Janus Spheres. *Science* **2011**, *331*, 199–202.
23. Mao, Z.; Xu, H.; Wang, D. Molecular Mimetic Self-Assembly of Colloidal Particles. *Adv. Funct. Mater.* **2010**, *20*, 1053–1074.
24. Li, F.; Josephson, D. P.; Stein, A. Colloidal Assembly: The Road from Particles to Colloidal Molecules and Crystals. *Angew. Chem., Int. Ed.* **2011**, *50*, 360–388.
25. Frenkel, D. Onsager's Spherocylinders Revisited. *J. Phys. Chem.* **1987**, *91*, 4912–4916.
26. Stroobants, A.; Lekkerkerker, H. N. W.; Frenkel, D. Evidence for One-, Two-, and Three-Dimensional Order in a System of Hard Parallel Spherocylinders. *Phys. Rev. A* **1987**, *36*, 2929–2945.
27. Schilling, T.; Pronk, S.; Mulder, B.; Frenkel, D. Monte Carlo Study of Hard Pentagons. *Phys. Rev. E* **2005**, *71*, 036138.
28. John, B. S.; Juhlin, C.; Escobedo, F. A. Phase Behavior of Colloidal Hard Perfect Tetragonal Parallelepipeds. *J. Chem. Phys.* **2008**, *128*, 044909.
29. Haji-Akbari, A.; Engel, M.; Keys, A. S.; Zheng, X.; Petschek, R. G.; Palffy-Muhoray, P.; Glotzer, S. C. Disordered, Quasicrystalline and Crystalline Phases of Densely Packed Tetrahedra. *Nature* **2009**, *462*, 773–777.
30. Evers, W. H.; Nijs, B. D.; Filion, L.; Castillo, S.; Dijkstra, M.; Vanmaekelbergh, D. Entropy-Driven Formation of Binary Semiconductor-Nanocrystal Superlattices. *Nano Lett.* **2010**, *10*, 4235–4241.
31. Agarwal, U.; Escobedo, F. A. Mesophase Behaviour of Polyhedral Particles. *Nat. Mater.* **2011**, *10*, 230–235.
32. Zhao, K.; Bruinsma, R.; Mason, T. G. Entropic Crystal–Crystal Transitions of Brownian Squares. *Proc. Natl. Acad. Sci. U. S.A.* **2011**, *108*, 2684–2687.
33. Haji-Akbari, A.; Engel, M.; Glotzer, S. C. Degenerate Quasicrystal of Hard Triangular Bipyramids. *Phys. Rev. Lett.* **2011**, *107*, 215702.
34. Rossi, L.; Sacanna, S.; Irvine, W. T. M.; Chaikin, P. M.; Pine, D. J.; Philipse, A. P. Cubic Crystals from Cubic Colloids. *Soft Matter* **2011**, *7*, 4139–4142.
35. Damasceno, P. F.; Engel, M.; Glotzer, S. C. Crystalline Assemblies and Densest Packings of a Family of Truncated Tetrahedra and the Role of Directional Entropic Forces. *ACS Nano* **2012**, *6*, 609–614.
36. Damasceno, P. F.; Engel, M.; Glotzer, S. C. Predictive Self-Assembly of Polyhedra into Complex Structures. *Science* **2012**, *337*, 453–457.
37. Henzie, J.; Grünwald, M.; Widmer-Cooper, A.; Geissler, P. L.; Yang, P. Self-Assembly of Uniform Polyhedral Silver Nanocrystals into Densest Packings and Exotic Superlattices. *Nat. Mater.* **2012**, *11*, 131–137.
38. Ni, R.; Gantapara, A. P.; de Graaf, J.; van Roij, R.; Dijkstra, M. Phase Diagram of Colloidal Hard Superballs: From Cubes *via* Spheres to Octahedra. *Soft Matter* **2012**, *8*, 8826–8834.
39. Zhang, J.; Luo, Z.; Martens, B.; Quan, Z.; Kumbhar, A.; Porter, N.; Wang, Y.; Smilgies, D.-M.; Fang, J. Reversible Kirkwood–Alder Transition Observed in Pt_3Cu_2 Nanoctahedron Assemblies under Controlled Solvent Annealing/Drying Conditions. *J. Am. Chem. Soc.* **2012**, *134*, 14043–14049.
40. Agarwal, U.; Escobedo, F. A. Effect of Quenched Size Polydispersity on the Ordering Transitions of Hard Polyhedral Particles. *J. Chem. Phys.* **2012**, *137*, 024905.
41. Smallenburg, F.; Filion, L.; Marechal, M.; Dijkstra, M. Vacancy-Stabilized Crystalline Order in Hard Cubes. *Proc. Natl. Acad. Sci. U.S.A.* **2012**, *109*, 17886–17890.
42. Marechal, M.; Patti, A.; Dennison, M.; Dijkstra, M. Frustration of the Isotropic-Columnar Phase Transition of Colloidal Hard Platelets by a Transient Cubatic Phase. *Phys. Rev. Lett.* **2012**, *108*, 206101.
43. Gantapara, A. P.; de Graaf, J.; van Roij, R.; Dijkstra, M. Phase Diagram and Structural Diversity of a Family of Truncated Cubes: Degenerate Close-Packed Structures and Vacancy-Rich States. *Phys. Rev. Lett.* **2013**, *111*, 015501.
44. Cademartiri, L.; Bishop, K. J. M.; Snyder, P. W.; Ozin, G. A. Using Shape for Self-Assembly. *Philos. Trans. R. Soc., A* **2012**, *370*, 2824–2847.
45. Young, K. L.; Personick, M. L.; Engel, M.; Damasceno, P. F.; Barnaby, S. N.; Bleher, R.; Li, T.; Glotzer, S. C.; Lee, B.; Mirkin, C. A. A Directional Entropic Force Approach To Assemble Anisotropic Nanoparticles into Superlattices. *Angew. Chem., Int. Ed.* **2013**, *52*, 13980–13984.
46. van Anders, G.; Ahmed, N. K.; Klotsa, D.; Engel, M.; Glotzer, S. C. Unified Theoretical Framework for Shape Entropy in Colloids. *arXiv:1309.1187*, **2013**.
47. Romano, F.; Sanz, E.; Sciortino, F. Role of the Range in the Fluid-Crystal Coexistence for a Patchy Particle Model. *J. Phys. Chem. B* **2009**, *113*, 15133–15136.
48. Sacanna, S.; Irvine, W. T. M.; Chaikin, P. M.; Pine, D. Lock and Key Colloids. *Nature* **2010**, *464*, 575–578.
49. Sacanna, S.; Korpics, M.; Rodriguez, K.; Colon-Melendez, L.; Kim, S.-H.; Pine, D. J.; Yi, G.-R. Shaping Colloids for Self-Assembly. *Nat. Commun.* **2013**, *4*, 1688.
50. Zhao, K.; Mason, T. G. Directing Colloidal Self-Assembly through Roughness-Controlled Depletion Attractions. *Phys. Rev. Lett.* **2007**, *99*, 268301.
51. Zhao, K.; Mason, T. G. Suppressing and Enhancing Depletion Attractions between Surfaces Roughened by Asperities. *Phys. Rev. Lett.* **2008**, *101*, 148301.
52. Badaire, S.; Cottin-Bizonne, C.; Woody, J. W.; Yang, A.; Stroock, A. D. Shape Selectivity in the Assembly of Lithographically Designed Colloidal Particles. *J. Am. Chem. Soc.* **2007**, *129*, 40–41.
53. Badaire, S.; Cottin-Bizonne, C.; Stroock, A. D. Experimental Investigation of Selective Colloidal Interactions Controlled by Shape, Surface Roughness, and Steric Layers. *Langmuir* **2008**, *24*, 11451–11463.
54. Yake, A. M.; Snyder, C. E.; Velegol, D. Site-Specific Functionalization on Individual Colloids: Size Control, Stability, and Multilayers. *Langmuir* **2007**, *23*, 9069–9075.
55. Snyder, C. E.; Ong, M.; Velegol, D. In-Solution Assembly of Colloidal Water. *Soft Matter* **2009**, *5*, 1263–1268.
56. Kraft, D. J.; Ni, R.; Smallenburg, F.; Hermes, M.; Yoon, K.; Weitz, D. A.; van Blaaderen, A.; Groenewold, J.; Dijkstra, M.; Kegel, W. K. Surface Roughness Directed Self-Assembly of Patchy Particles into Colloidal Micelles. *Proc. Natl. Acad. Sci. U.S.A.* **2012**, *109*, 10787–10792.
57. Ahmadi, T. S.; Wang, Z. L.; Green, T. C.; Henglein, A.; El-Sayed, M. A. Shape-Controlled Synthesis of Colloidal Platinum Nanoparticles. *Science* **1996**, *272*, 1924–1925.
58. Sau, T. K.; Murphy, C. J. Room Temperature, High-Yield Synthesis of Multiple Shapes of Gold Nanoparticles in Aqueous Solution. *J. Am. Chem. Soc.* **2004**, *126*, 8648–8649.
59. Demortière, A.; Launois, P.; Goubet, N.; Albouy, P.-A.; Petit, C. Shape-Controlled Platinum Nanocubes and Their Assembly into Two-Dimensional and Three-Dimensional Superlattices. *J. Phys. Chem. B* **2008**, *112*, 14583–14592.
60. Seo, D.; Park, J. C.; Song, H. Polyhedral Gold Nanocrystals with OH Symmetry: From Octahedra to Cubes. *J. Am. Chem. Soc.* **2006**, *128*, 14863–14870.
61. Fan, F.-R.; Liu, D.-Y.; Wu, Y.-F.; Duan, S.; Xie, Z.-X.; Jiang, Z.-Y.; Tian, Z.-Q. Epitaxial Growth of Heterogeneous Metal Nanocrystals: From Gold Nano-octahedra to Palladium and Silver Nanocubes. *J. Am. Chem. Soc.* **2008**, *130*, 6949–6951.
62. Habas, S. E.; Lee, H.; Radmilovic, V.; Somorjai, G. A.; Yang, P. Shaping Binary Metal Nanocrystals through Epitaxial Seeded Growth. *Nat. Mater.* **2007**, *6*, 692–697.
63. Song, H.; Kim, F.; Connor, S.; Somorjai, G. A.; Yang, P. Pt Nanocrystals: Shape Control and Langmuir–Blodgett

Monolayer Formation. *J. Phys. Chem. B* **2005**, *109*, 188–193.
64. Skrabalak, S. E.; Au, L.; Li, X.; Xia, Y. Facile Synthesis of Ag Nanocubes and Au Nanocages. *Nat. Protoc.* **2007**, 2182–2190.
65. Jana, N. R.; Gearheart, L.; Murphy, C. J. Wet Chemical Synthesis of Silver Nanorods and Nanowires of Controllable Aspect Ratio. *Chem. Commun.* **2001**, 617–618.
66. Kim, F.; Connor, S.; Song, H.; Kuykendall, T.; Yang, P. Platonic Gold Nanocrystals. *Angew. Chem., Int. Ed.* **2004**, *43*, 3673–3677.
67. Klajn, R.; Pinchuk, A.; Schatz, G.; Grzybowski, B. Synthesis of Heterodimeric Sphere-Prism Nanostructures *via* Metastable Gold Supraspheres. *Angew. Chem., Int. Ed.* **2007**, *46*, 8363–8367.
68. Tian, N.; Zhou, Z.-Y.; Sun, S.-G.; Ding, Y.; Wang, Z. L. Synthesis of Tetrahexahedral Platinum Nanocrystals with High-Index Facets and High Electro-oxidation Activity. *Science* **2007**, *316*, 732–735.
69. Murphy, C. J.; Sau, T. K.; Gole, A. M.; Orendorff, C. J.; Gao, J.; Gou, L.; Hunyadi, S. E.; Li, T. Anisotropic Metal Nanoparticles: Synthesis, Assembly, and Optical Applications. *J. Phys. Chem. B* **2005**, *109*, 13857–13870.
70. Grzelczak, M.; Perez-Juste, J.; Mulvaney, P.; Liz-Marzan, L. M. Shape Control in Gold Nanoparticle Synthesis. *Chem. Soc. Rev.* **2008**, *37*, 1783–1791.
71. Zhao, N.; Ma, W.; Cui, Z.; Song, W.; Xu, C.; Gao, M. Polyhedral Maghemite Nanocrystals Prepared by a Flame Synthetic Method: Preparations, Characterizations, and Catalytic Properties. *ACS Nano* **2009**, *3*, 1775–1780.
72. Ho, C.; Keller, A.; Odell, J.; Ottewill, R. Preparation of Monodisperse Ellipsoidal Polystyrene Particles. *Colloid Polym. Sci.* **1993**, *271*, 469–479.
73. Clark, T. D.; Tien, J.; Duffy, D. C.; Paul, K. E.; Whitesides, G. M. Self-Assembly of 10-μm-Sized Objects into Ordered Three-Dimensional Arrays. *J. Am. Chem. Soc.* **2001**, *123*, 7677–7682.
74. Velikov, K. P.; van Dillen, T.; Polman, A.; van Blaaderen, A. Photonic Crystals of Shape-Anisotropic Colloidal Particles. *Appl. Phys. Lett.* **2002**, *81*, 838–840.
75. van Dillen, T.; Polman, A.; van Kats, C. M.; van Blaaderen, A. Ion Beam-Induced Anisotropic Plastic Deformation at 300 keV. *Appl. Phys. Lett.* **2003**, *83*, 4315–4317.
76. Mohraz, A.; Solomon, M. J. Direct Visualization of Colloidal Rod Assembly by Confocal Microscopy. *Langmuir* **2005**, *21*, 5298–5306.
77. Hernandez, C. J.; Mason, T. G. Colloidal Alphabet Soup: Monodisperse Dispersions of Shape-Designed Lithoparticles. *J. Phys. Chem. C* **2007**, *111*, 4477–4480.
78. Moon, J.; Kim, A.; Crocker, J.; Yang, S. High-Throughput Synthesis of Anisotropic Colloids *via* Holographic Lithography. *Adv. Mater.* **2007**, *19*, 2508–2512.
79. Champion, J. A.; Katare, Y. K.; Mitragotri, S. Making Polymeric Micro- and Nanoparticles of Complex Shapes. *Proc. Natl. Acad. Sci. U.S.A.* **2007**, *104*, 11901–11904.
80. Yanai, N.; Granick, S. Directional Self-Assembly of a Colloidal Metal-Organic Framework. *Angew. Chem.* **2012**, *124*, 5736–5739.
81. Tao, A.; Sinsermsuksakul, P.; Yang, P. Tunable Plasmonic Lattices of Silver Nanocrystals. *Nat. Nanotechnol.* **2007**, *2*, 435–440.
82. Zhang, L.; Feng, G.; Zeravcic, Z.; Brugarolas, T.; Liu, A. J.; Lee, D. Using Shape Anisotropy To Toughen Disordered Nanoparticle Assemblies. *ACS Nano* **2013**, *7*, 8043–8050.
83. Fernandes, B. D.; Spuch-Calvar, M.; Baida, H.; Tréguer-Delapierre, M.; Oberlé, J.; Langot, P.; Burgin, J. Acoustic Vibrations of Au Nano-bipyramids and Their Modification under Ag Deposition: A Perspective for the Development of Nanobalances. *ACS Nano* **2013**, *7*, 7630–7639.
84. Sau, T. K.; Rogach, A. L. Nonspherical Noble Metal Nanoparticles: Colloid-Chemical Synthesis and Morphology Control. *Adv. Mater.* **2010**, *22*, 1781–1804.
85. Xia, Y.; Xiong, Y.; Lim, B.; Skrabalak, S. Shape-Controlled Synthesis of Metal Nanocrystals: Simple Chemistry Meets Complex Physics? *Angew. Chem., Int. Ed.* **2009**, *48*, 60–103.
86. Désert, A.; Hubert, C.; Fu, Z.; Moulet, L.; Majimel, J.; Barboteau, P.; Thill, A.; Lansalot, M.; Bourgeat-Lami, E.; Duguet, E.; *et al.* Synthesis and Site-Specific Functionalization of Tetravalent, Hexavalent, and Dodecavalent Silica Particles. *Angew. Chem., Int. Ed.* **2013**, *52*, 11068–11072.
87. Odriozola, G.; Jimenez-Angeles, F.; Lozada-Cassou, M. Entropy Driven Key-Lock Assembly. *J. Chem. Phys.* **2008**, *129*, 111101.
88. König, P.-M.; Roth, R.; Dietrich, S. Lock and Key Model System. *Europhys. Lett.* **2008**, *84*, 68006.
89. Odriozola, G.; Lozada-Cassou, M. Statistical Mechanics Approach to Lock−Key Supramolecular Chemistry Interactions. *Phys. Rev. Lett.* **2013**, *110*, 105701.
90. Sacanna, S.; Pine, D. J. Shape-Anisotropic Colloids: Building Blocks for Complex Assemblies. *Curr. Opin. Colloid Interface Sci.* **2011**, *16*, 96–105.
91. Iacovella, C. R.; Rogers, R. E.; Glotzer, S. C.; Solomon, M. J. Pair Interaction Potentials of Colloids by Extrapolation of Confocal Microscopy Measurements of Collective Suspension Structure. *J. Chem. Phys.* **2010**, *133*, 164903.
92. Royall, C. P.; Poon, W. C. K.; Weeks, E. R. In Search of Colloidal Hard Spheres. *Soft Matter* **2013**, *9*, 17–27.
93. Young, K. L.; Jones, M. R.; Zhang, J.; Macfarlane, R. J.; Esquivel-Sirvent, R.; Nap, R. J.; Wu, J.; Schatz, G. C.; Lee, B.; Mirkin, C. A. Assembly of Reconfigurable One-Dimensional Colloidal Superlattices Due to a Synergy of Fundamental Nanoscale Forces. *Proc. Natl. Acad. Sci. U.S.A.* **2012**, *109*, 2240–2245.
94. Ye, X.; Jun, C.; Engel, M.; Millan, J. A.; Li, W.; Qi, L.; Xing, G.; Collins, J. E.; Kagan, C. R.; Li, J.; *et al.* Competition of Shape and Interaction Patchiness for Self-Assembling Nanoplates. *Nat. Chem.* **2013**, *5*, 466–473.
95. Tang, Z.; Zhang, Z.; Wang, Y.; Glotzer, S. C.; Kotov, N. A. Self-Assembly of CdTe Nanocrystals into Free-Floating Sheets. *Science* **2006**, *314*, 274–278.
96. Gilbert, E.; Johnson, D.; Keerthi, S. A Fast Procedure for Computing the Distance between Complex Objects in Three-Dimensional Space. *IEEE J. Rob. Autom.* **1988**, *4*, 193–203.